The Astrophysical Journal, 782:3 (7pp), 2014 February 10 doi:10.1088/0004-637X/782/1/3

NuSTAR AND *SWIFT* OBSERVATIONS OF THE FAST ROTATING MAGNETIZED WHITE DWARF AE AQUARII

Takao Kitaguchi[1], Hongjun An[2], Andrei M. Beloborodov[3], Eric V. Gotthelf[3], Takayuki Hayashi[4], Victoria M. Kaspi[2], Vikram R. Rana[5], Steven E. Boggs[6], Finn E. Christensen[7], William W. Craig[6,8], Charles J. Hailey[3], Fiona A. Harrison[5], Daniel Stern[9], and Will W. Zhang[10]

[1] RIKEN Nishina Center, 2-1 Hirosawa, Wako, Saitama 351-0198, Japan
[2] Department of Physics, McGill University, Rutherford Physics Building, 3600 University Street, Montreal, Quebec H3A 2T8, Canada
[3] Physics Department and Columbia Astrophysics Laboratory, Columbia University, New York, NY 10027, USA
[4] The Institute of Space and Astronautical Science/JAXA, 3-1-1 Yoshinodai, Chuo-ku, Sagamihara 252-5210, Japan
[5] Cahill Center for Astronomy and Astrophysics, California Institute of Technology, Pasadena, CA 91125, USA
[6] Space Sciences Laboratory, University of California, Berkeley, CA 94720, USA
[7] DTU Space-National Space Institute, Technical University of Denmark, Elektrovej 327, DK-2800 Lyngby, Denmark
[8] Lawrence Livermore National Laboratory, Livermore, CA 94550, USA
[9] Jet Propulsion Laboratory, California Institute of Technology, Pasadena, CA 91109, USA
[10] NASA Goddard Space Flight Center, Greenbelt, MD 20771, USA

Received 2013 October 31; accepted 2013 December 17; published 2014 January 17

ABSTRACT

AE Aquarii is a cataclysmic variable with the fastest known rotating magnetized white dwarf ($P_{\rm spin} = 33.08$ s). Compared to many intermediate polars, AE Aquarii shows a soft X-ray spectrum with a very low luminosity ($L_{\rm X} \sim 10^{31}$ erg s^{-1}). We have analyzed overlapping observations of this system with the *NuSTAR* and the *Swift* X-ray observatories in 2012 September. We find the 0.5–30 keV spectra to be well fitted by either an optically thin thermal plasma model with three temperatures of $0.75^{+0.18}_{-0.45}$, $2.29^{+0.96}_{-0.82}$, and $9.33^{+6.07}_{-2.18}$ keV, or an optically thin thermal plasma model with two temperatures of $1.00^{+0.34}_{-0.23}$ and $4.64^{+1.58}_{-0.84}$ keV plus a power-law component with photon index of $2.50^{+0.17}_{-0.23}$. The pulse profile in the 3–20 keV band is broad and approximately sinusoidal, with a pulsed fraction of $16.6\% \pm 2.3\%$. We do not find any evidence for a previously reported sharp feature in the pulse profile.

Key words: accretion, accretion disks – novae, cataclysmic variables – stars: individual (AE Aquarii) – white dwarfs – X-rays: stars

Online-only material: color figures

1. INTRODUCTION

AE Aquarii (hereafter AE Aqr) is a cataclysmic variable binary system classified as a member of the DQ Herculis or intermediate polar (IP) class (Patterson 1994). It is a non-eclipsing close binary system at a distance of 102^{+42}_{-23} pc (Friedjung 1997), consisting of a magnetic white dwarf (primary) and a K4–5 V star (secondary) with an orbital period, $P_{\rm orbit} = 9.88$ hr. The 33.08 s period makes AE Aqr the fastest-spinning magnetic white dwarf. The pulsations were originally discovered in the optical (Patterson 1979), then confirmed in soft X-rays (Patterson et al. 1980) and the ultraviolet (Eracleous et al. 1994). In the DQ Herculis class, the white dwarf is generally thought to possess a magnetic field ($B \sim 10^{5-7}$ G) strong enough to channel the accretion flow from the secondary to the poles of the white dwarf. Accordingly, hard X-rays are produced by the shock-heated gas, which reaches temperatures of a few tens of keV near the surface. The white dwarf photosphere, heated by the hard X-rays, emits ultraviolet light. These emissions exhibit spin modulation caused by the varying aspect of the accreting poles as the white dwarf rotates (see Patterson 1994 for a review).

AE Aqr stands out as an unusual member of the DQ Herculis class. It displays strong flares of broad-band emission, from radio to X-rays. In addition, possible TeV γ-ray flares have been reported (Meintjes et al. 1994), although they have not yet been confirmed with more recent TeV Cerenkov telescopes (Mauche et al. 2012). The persistent X-ray luminosity of AE Aqr ($\sim 10^{31}$ erg s^{-1}) is two orders of magnitude lower than that of typical IPs. Its X-ray spectrum has been modeled as emission from an optically thin thermal plasma with several temperature components, similar to those seen from other IPs. However, the highest temperature found in such models was 4.6 keV (Itoh et al. 2006), which is significantly lower than the average $kT \approx 22$ keV found in the 22 IPs detected by *INTEGRAL* (Landi et al. 2009). For these reasons, the mechanism and location of the X-ray emission are still uncertain (e.g., Choi et al. 1999; Itoh et al. 2006; Mauche 2009).

Another intriguing feature reported by a *Suzaku* observation in 2005 is that AE Aqr may emit non-thermal hard X-rays with a very narrow pulse profile at the spin period (Terada et al. 2008), suggesting that AE Aqr may accelerate charged particles in a fashion similar to rotation-powered pulsars (e.g., Kaspi et al. 2006 for a review). However, the *Suzaku* observation in 2006 did not reproduce the earlier result, leaving the detection of non-thermal X-rays from AE Aqr uncertain.

In this paper, we present broad-band X-ray observations of AE Aqr obtained with *NuSTAR* and *Swift*. Section 2 details the observations, data reduction, and background modeling. These more sensitive observations in the hard X-ray band can help measure the maximum temperature of the thermal plasma in AE Aqr and test the presence of any beamed non-thermal component. We describe the spectral modeling in Section 3 and the timing analysis in Section 4. The results and a possible interpretation are discussed in Section 5. Throughout this paper, all errors are given at the 90% confidence level unless otherwise stated.

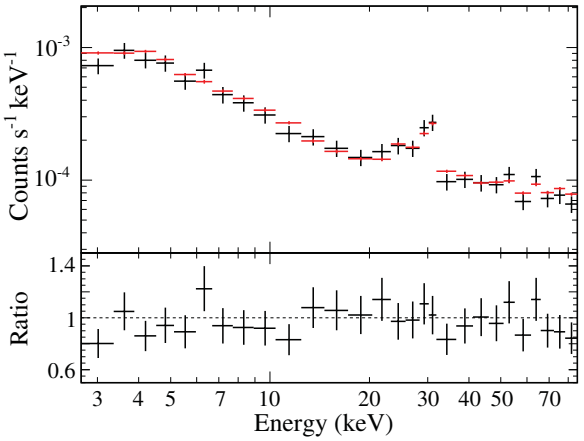

Figure 1. Comparison of (red) the background model produced by `nuskybgd` with (black) the actual blank-sky spectrum in the AE Aqr observation. The bottom panel shows the spectral ratio of the actual data to the model.

(A color version of this figure is available in the online journal.)

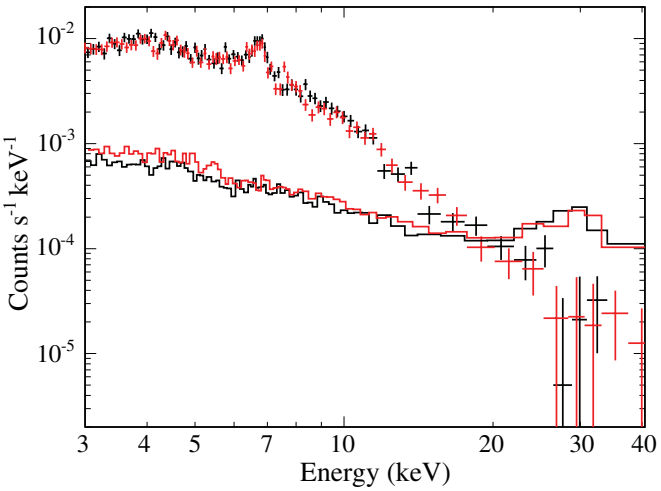

Figure 2. X-ray spectra of AE Aqr observed with the two *NuSTAR* telescopes, (black) FPMA and (red) FPMB. The cross points and solid histograms are the background-subtracted spectra and background models, respectively.

(A color version of this figure is available in the online journal.)

2. OBSERVATIONS AND DATA REDUCTIONS

2.1. NuSTAR

2.1.1. Observation Log and Data Screening

We observed AE Aqr with *NuSTAR* (Harrison et al. 2013), the first focusing hard X-ray (3–79 keV) telescopes in orbit, from 2012 September 4, 19:20 UT to September 7, 18:50 UT. *NuSTAR* was operated in its default mode throughout the observation. The acquired data with the observation ID of 30001120 were processed and screened in the standard way using the *NuSTAR* pipeline software, NuSTARDAS version 1.1.1, with the *NuSTAR* calibration database (CALDB) version 20130509. The data were filtered for intervals of high background, including Earth occultations and South Atlantic Anomaly (SAA) passages. This resulted in a total of 125 ks of dead-time corrected exposure time.

All photon arrival times were corrected to the solar system barycenter using the JPL DE200 ephemeris and the *Chandra* -derived coordinates (20:40:09.185, −00:52:15.08; J2000) which have sub-arcsecond uncertainties. The source photons were extracted from a circular region of radius 1.′0 centered on AE Aqr. The source spectra were grouped with a minimum of 50 counts per bin. The background spectra were generated with the background modeling tool, `nuskybgd` (D. R. Wik et al. in preparation). A detailed description of the background modeling is given in Section 2.1.2. The telescope response files, ARF and RMF were also generated by NuSTARDAS.

2.1.2. Background Spectral Modeling

Since AE Aqr is a faint source in hard X-rays, the *NuSTAR* background spectrum must be carefully subtracted from the source spectrum. Blank-sky observations show the background rate varies in an energy dependent way with detector position by a factor of ∼2 (Harrison et al. 2013). In addition, the internal background rate varies in time due to changes in the cosmic radiation intensity associated with the geomagnetic cutoff rigidity, as well as the elapsed time since SAA passage.

In order to perform accurate background subtraction, the background spectrum was empirically modeled using the *NuSTAR* background fitting and modeling tool, `nuskybgd` (revision 52). `nuskybgd` fits blank-sky spectra in user-selected regions of the same observation, and then generates a background spectrum within any regions with the best-fit parameters (Wik et al. in preparation for a more detailed).

Three blank-sky spectra for each telescope were extracted from annular regions of radius 120″–270″, 270″–370″, and 370″–740″ centered on AE Aqr to model the background spectra of the two *NuSTAR* telescopes. The blank-sky spectra were well fitted by the model with $\chi^2/\mathrm{dof} = 1217.6/1124$. The background count spectrum in the source region was modeled with an exposure 20 times longer than the actual one to reduce statistical errors. In order to verify the background model, the background spectrum in a blank-sky region 3.′5 from the source in a northeasterly direction was simulated and compared to the actual spectrum extracted from the same region. The ratio of the actual spectrum to the model in Figure 1 was fitted by a constant factor of 0.98 ± 0.04 with $\chi^2/\mathrm{dof} = 15.7/27$, showing the background model is consistent with the actual spectrum within statistical errors.

Figure 2 shows the AE Aqr spectra obtained with the two *NuSTAR* hard X-ray telescopes (FPMA and FPMB) and the background models. The highly ionized iron line can be seen around 6.7 keV. The total count rate in the 3–30 keV energy band after the background subtraction and dead-time correction is $(9.2 \pm 0.1) \times 10^{-2}$ counts s^{-1}.

2.2. Swift

Swift (Gehrels et al. 2004) observed AE Aqr simultaneously with *NuSTAR* from 2012 September 6, 06:07 to 07:53 UT. The *Swift* X-ray telescope (XRT; Burrows et al. 2005) was operated in the photon counting mode during the observation. The XRT data (observation ID 00030295037) were processed in the standard manner with xrtpipeline (ver. 0.12.6) in HEASoft (ver. 6.13). The total exposure time after the data screening is 1.54 ks. The source photons were extracted from a circular region of radius 1.′2 centered on AE Aqr. The source spectrum was rebinned to have at least 20 counts per bin. The background spectrum was extracted from an annular region of radius 1.′7–7.′0 centered on the source and was scaled by an area ratio of the source region to the background region.

Table 1
Best-fit Parameters of the Three-temperature Model

Parameter	Unit	Value
$N_{\rm H}$	(10^{20} cm^{-2})	<82.2
Z	($Z_{\odot}$[a])	$0.76^{+0.17}_{-0.13}$
kT_1	(keV)	$0.75^{+0.18}_{-0.45}$
F_1[b]	(10^{-12} erg s^{-1} cm^{-2})	$1.97^{+0.94}_{-0.85}$
kT_2	(keV)	$2.29^{+0.96}_{-0.82}$
F_2[b]	(10^{-12} erg s^{-1} cm^{-2})	$3.53^{+0.55}_{-0.64}$
kT_3	(keV)	$9.33^{+6.07}_{-2.18}$
F_3[b]	(10^{-12} erg s^{-1} cm^{-2})	$2.26^{+0.99}_{-0.96}$
$C_{\rm FPMB}/C_{\rm FPMA}$[c]		1.00 ± 0.03
$C_{\rm XRT}/C_{\rm FPMA}$[d]		$0.94^{+0.19}_{-0.22}$
χ^2/dof		247.1/201

Notes.
[a] Solar abundance from Wilms et al. (2000), in which the solar iron abundance relative to hydrogen is 2.69×10^{-5}. Note that the solar abundance from Anders & Grevesse (1989), in which the solar iron abundance is 4.68×10^{-5}, is employed in other AE Aqr articles (e.g., Itoh et al. 2006; Terada et al. 2008; Oruru & Meintjes 2012).
[b] Unabsorbed flux in 0.5–10 keV.
[c] Cross-normalization factor between *NuSTAR*/FPMB and *NuSTAR*/FPMA.
[d] Cross-normalization factor between *Swift*/XRT and *NuSTAR*/FPMA.

3. SPECTRAL ANALYSIS

3.1. Spectral Fitting with Multi-temperature Models

The X-ray spectra of AE Aqr observed with *ASCA* (Choi et al. 1999), *XMM-Newton* (Itoh et al. 2006), and *Suzaku* (Terada et al. 2008) have been modeled using an optically thin thermal plasma emission model with a few different temperature components in the same way as for other IPs. Therefore in the joint fitting of *Swift* and *NuSTAR* spectra, we adopted an emission model from a collisionally ionized diffuse plasma, `APEC` (Smith et al. 2001). Each `APEC` model was constrained to have common metal abundances relative to solar from Wilms et al. (2000), but was allowed to have different temperatures and normalizations. We use the `tbabs` model (Wilms et al. 2000) to account for interstellar and self-absorption. In addition, the cross-normalization factors of XRT/FPMA and FPMB/FPMA were allowed to vary.

In order to determine the number of `APEC` components with different temperatures, we added new `APEC` components one by one until the fit was not significantly improved, as determined by the *F*-test. Improvement of the fit is significant with the chance probability of $\ll1\%$ until the number of components is increased to three, whereas little improvement was found by the addition of a fourth component with the chance probability of 8.4% derived from the χ^2 reduction from 247.1 (dof = 201) to 241.0 (dof = 199). The 0.5–30 keV spectra of *Swift* and *NuSTAR* with the best-fit three-temperature `APEC` models are shown in Figure 3(a), the parameters of which are listed in Table 1. with previous results for reference. The highest temperature, $9.3^{+6.1}_{-2.2}$ keV, is considerably higher than previously observed for this source (4.6 keV from Itoh et al. 2006), and approaches the average temperature of 22 keV for any other IPs (Landi et al. 2009). The metal abundance, $0.76^{+0.17}_{-0.13}$ $Z_{\odot}$, is consistent with that determined by *XMM-Newton* and *Suzaku*. The total luminosity in 0.5–10 keV is $9.3^{+1.0}_{-2.2}\times10^{30}$ erg s^{-1} for an assumed distance of 100 pc.

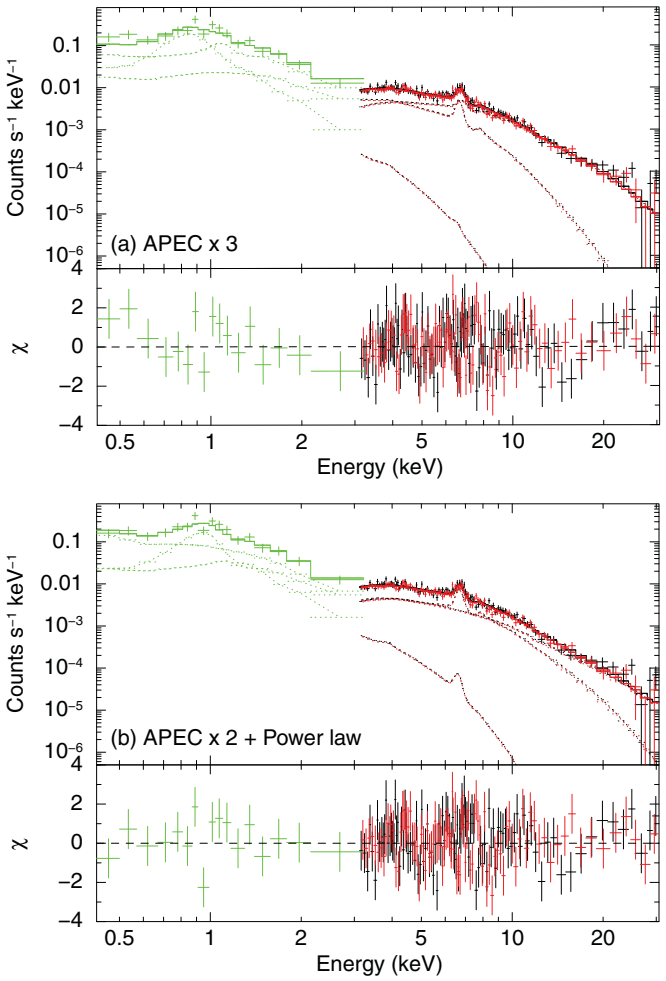

Figure 3. X-ray spectra of (green) *Swift*/XRT, (black) *NuSTAR*/FPMA, and (red) *NuSTAR*/FPMB overlaid with (a) the best-fit three-temperature `APEC` model and (b) two-temperature model with a power-low emission. The model components are drawn with dotted lines. The bottom panels show fit residuals in terms of σ with error bars of size one.
(A color version of this figure is available in the online journal.)

Although other IP spectra commonly contain a strong neutral (or low-ionized) iron line around 6.4 keV with a comparable equivalent width to highly ionized iron emission around 6.7 keV (e.g., Ezuka & Ishida 1999; Yuasa et al. 2010), we do not detect this feature clearly in the AE Aqr spectrum. In fact, *XMM-Newton* spectra constrained the upper limit to the 6.4 keV equivalent width to be <61 eV (Itoh et al. 2006). We tried to add a narrow Gaussian emission model with a center energy fixed at 6.4 keV to the three-temperature `APEC` model, and simultaneously fit the spectra of *Swift* and *NuSTAR* with it. The intensity of the neutral iron line is $1.33^{+1.26}_{-1.33}\times10^{-14}$ erg s^{-1} cm^{-2}, which corresponds to an equivalent width of $37.9^{+41.7}_{-37.9}$ eV. On the other hand, the intensity of the highly ionized iron line around 6.7 keV was determined to be $1.11^{+0.11}_{-0.09}\times10^{-13}$ erg s^{-1} cm^{-2}, or an equivalent width of 495^{+365}_{-53} eV, with the line central energy of $6.732^{+0.063}_{-0.014}$ keV. Therefore, the neutral iron line is much weaker than the highly ionized iron line.

3.2. Spectral Fitting with Non-thermal Emission

In order to search for possible non-thermal hard X-rays as suggested by Terada et al. (2008), we simultaneously fitted the spectra of *Swift* and *NuSTAR* with a multi-temperature

Table 2
Best-fit Parameters of the Two-temperature Model with Power-law Emission

Parameter	Unit	Value
$N_{\rm H}$	(10^{20} cm^{-2})	<82.2
Z	($Z_\odot$)	$1.14^{+0.62}_{-0.33}$
kT_1	(keV)	$1.00^{+0.34}_{-0.23}$
F_1[a]	(10^{-12} erg s^{-1} cm^{-2})	$2.01^{+1.25}_{-1.03}$
kT_2	(keV)	$4.64^{+1.58}_{-0.84}$
F_2[a]	(10^{-12} erg s^{-1} cm^{-2})	$1.86^{+0.96}_{-0.81}$
Γ		$2.50^{+0.17}_{-0.23}$
$F_{\rm PL}$[b]	(10^{-12} erg s^{-1} cm^{-2})	$4.07^{+1.66}_{-1.50}$
$C_{\rm FPMB}/C_{\rm FPMA}$		1.00 ± 0.03
$C_{\rm XRT}/C_{\rm FPMA}$		$0.81^{+0.22}_{-0.19}$
χ^2/dof		244.5/201

Notes.
[a] Unabsorbed flux of each thermal emission component in 0.5–10 keV.
[b] Unabsorbed flux of the power-law model in 0.5–10 keV.

plus power-law emission model. In the same way as the determination of the number of APEC components described above, we first fit the spectra using a single APEC with a power-law model, and then added new APEC models one by one until the fit was not significantly improved as determined by the F-test. We find two temperatures with power-law emission is the statistically favored model.

The *Swift* and *NuSTAR* spectra with the best-fit model are shown in Figure 3(b), the parameters of which are listed in Table 2. Compared with the three-temperature APEC model, the fit with the two-APEC model with the power-law emission is slightly but not significantly preferred. We cannot distinguish whether the hard X-ray component detected with *NuSTAR* is thermal or non-thermal emission.

4. TIMING ANALYSIS

4.1. Spin Period Determination

We examined the hard X-ray pulse profile for evidence of the narrow pulsation reported by *Suzaku* (Terada et al. 2008). Previous measurements have shown that soft X-rays below 10 keV are sinusoidally modulated with a single peak in the spin phase of the white dwarf (e.g., Mauche 2006). In this case, the Z_1^2-statistic, or Rayleigh test (Buccheri et al. 1983) is more sensitive to determine the spin period than the epoch folding technique with the χ^2 test (Leahy et al. 1983).

Figure 4(a) shows the Z_1^2 periodogram using *NuSTAR* 3–10 keV data with barycenter-corrected time. We found the peak at 33.0769 ± 0.0004 s with $Z_1^2 = 124.1$. Within the uncertainty, the period is consistent with previously measured values in the optical band (Patterson 1979; de Jager et al. 1994), and at X-ray energies (Choi et al. 1999; Choi & Dotani 2006; Mauche 2006; Terada et al. 2008; Oruru & Meintjes 2012).

We also searched for a signal in the 10–20 keV energy band. The hard X-rays above 20 keV were ignored to improve the signal-to-noise ratio since the source rate from AE Aqr falls below that of the background in that energy range (Figure 2). Evidence for a pulsation was found also in this band at the expected pulse period, 33.0765 ± 0.0016 s, with $Z_1^2 = 11.1$, corresponding to a null hypothesis probability of 0.38%, or 2.9σ detection significance (Figure 4(b)).

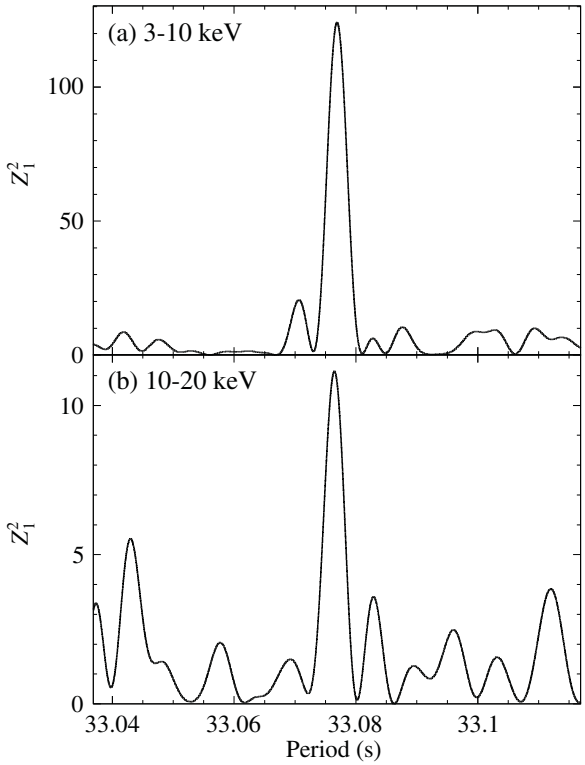

Figure 4. Z_1^2 periodograms acquired with *NuSTAR* in the energy bands of (a) 3–10 and (b) 10–20 keV.

Table 3
Pulse Profile Parameters[a] for AE Aqr

Energy Range (keV)	Peak Phase[b]	Pulse Fraction (%)	χ^2/dof
3–20	0.30 ± 0.02	16.6 ± 2.3	17.2/16
3–6	0.31 ± 0.04	14.8 ± 3.1	11.7/10
6–10	0.31 ± 0.03	19.9 ± 3.7	8.4/10
10–20	0.22 ± 0.10	14.2 ± 8.0	2.5/4

Notes.
[a] Best-fit parameters for a fit to the *NuSTAR* pulse profiles presented in Figure 5 using a sinusoid model with a constant offset, C: $C(1.0 + f_{\rm P}\cos(2\pi(\phi - \phi_0)))$, where ϕ_0 is the peak phase and $f_{\rm P}$ is the pulse fraction.
[b] Phase 0 corresponds to that of Figure 5.

4.2. Pulse Profile

Figure 5 presents the pulse profiles in several energy bands, folded on the best determined period, with the background subtracted using the model of Section 2.1.2. The profiles are well represented by sinusoidal functions (see Table 3). We find no evidence for significant variation in the phase or relative modulation amplitude (or pulse fraction) with energy. The mean pulse fraction, $16.6\% \pm 2.3\%$, is consistent with that found in the quiescent phase from *XMM-Newton* observations (Itoh et al. 2006; Choi & Dotani 2006).

We searched for a narrow peak in the pulse profile as reported by Terada et al. (2008) based on the *Suzaku* observation of 2005. We investigated the pulse profile using different numbers of bins per cycle ranging from 5 to 50. Furthermore, we examined the profile using 29 bins per cycle as per the *Suzaku* analysis and reproduced 1000 pulse profiles, each having a different start time at phase zero. Then we looked for any significant outliers

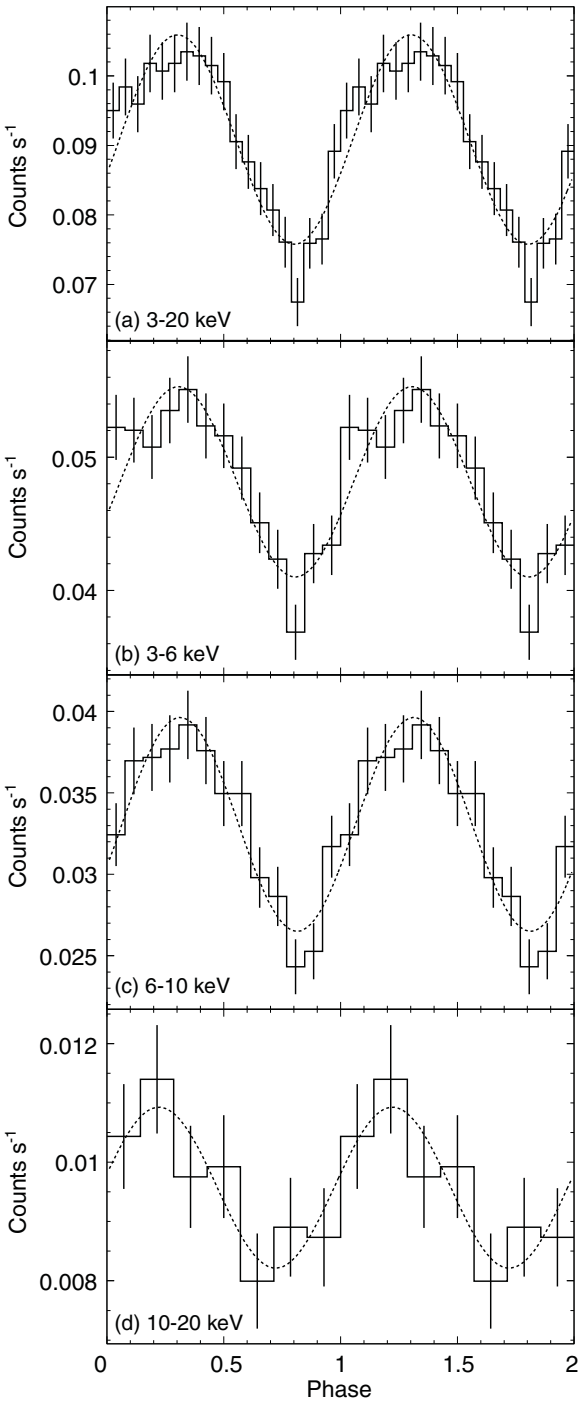

Figure 5. AE Aqr pulse profiles folded on the best period of 33.0769 s in (a) 3–20, (b) 3–6, (c) 6–10, and (d) 10–20 keV energy bands. The dashed curves show the best-fit sinusoidal models. The epoch of phase 0 corresponds to 56174.5 in MJD.

from the sinusoidal model with a 95% confidence level. We conclude that there is no evidence for an additional sharp pulse component in our data.

5. DISCUSSION

5.1. Comparison of Non-thermal Hard X-Ray Emission with Previous Suzaku Results

The 10–30 keV flux determined with *NuSTAR* is $5.0^{+1.3}_{-1.4} \times 10^{-13}$ erg s^{-1} cm^{-2}, about half of the best-fit *Suzaku*/HXD-PIN flux in 2005 (Terada et al. 2008). The derived power-law index, 2.5 ± 0.2, is also inconsistent with the *Suzaku* value, 1.1 ± 0.6, and is steeper than those found for rotation-powered pulsars, which range from 0.6 to 2.1 (Gotthelf 2003; Kaspi et al. 2006). Here we note that the previously reported *Suzaku* fitting errors did not include the systematic uncertainty of the *Suzaku*/HXD-PIN background model because the authors described that the hard X-ray flux was consistent with the narrow pulse flux in the spin profile. However, the systematic uncertainty, 3% (Fukazawa et al. 2009), is comparable to the background-subtracted count rate, and therefore should not be ignored (see Figures 6 and 7 of Terada et al. 2008 for comparison of the rates). It is possible that the discrepancy of the non-thermal emission parameters is due to the neglected systematic error in Terada et al. (2008).

Furthermore, we find no evidence of the narrow pulse profile with a pulse fraction of nearly 100% and a duty cycle of ∼0.1 reported by Terada et al. (2008). In contrast with the *Suzaku* result, we marginally detect the sinusoidal modulation in the 10–20 keV energy band at a significance level of 2.9σ. In order to determine whether or not *NuSTAR* is sensitive to the narrow pulse profile suggested by *Suzaku*, we estimated its count rate considering the *NuSTAR* telescope response and assuming the *Suzaku* result. The expected 10–20 keV count rate within a duty cycle of 0.1 is 0.086 ± 0.003 count s^{-1}, 10 times higher than the time-averaged rate measured with *NuSTAR*, indicating that *NuSTAR* would have been capable of significantly detecting the narrow pulsation.

A possible explanation of the difference between the *Suzaku* and *NuSTAR* results is that AE Aqr may have varied and its hard X-ray flux decreased. However, the soft X-ray flux determined with *NuSTAR* in 2012 is consistent with previous observations made with *Suzaku* in 2005 (see Table 1), within the cross-normalization factor of *NuSTAR* to *Suzaku*/XIS of ∼15% (based on simultaneous observations of calibration targets). It is difficult to explain a mechanism only in hard X-rays that would make the flux vary without correlation of thermal soft X-rays, a part of which also modulates with the spin period.

5.2. Possible Interpretation of the Observed Emission

Two energy sources could, in principle, power the observed X-ray luminosity $L_X \sim 10^{31}$ erg s^{-1}: liberation of gravitational energy of accreting matter and the rotational energy of the white dwarf.

The white dwarf was reported to spin down with a rate $\dot{P} = 5.64 \times 10^{-14}$ s s^{-1} (de Jager et al. 1994), which corresponds to spindown power $L_{\rm sd} \sim 10^{34}$ erg s^{-1} $\gg L_X$. This suggests the possibility that the X-ray emission of the white dwarf is fed by rotation (Ikhsanov & Beskrovnaya 2012). The rotation-induced electric field could accelerate particles to high Lorentz factors if the magnetosphere is plasma-starved and the electric field is not screened. Synchrotron emission was suggested as a possible radiative mechanism in such a model (Terada et al. 2008). It is, however, unclear how the observed luminosity, spectrum, and pulse profile observed by *NuSTAR* would be produced by relativistic particles. The efficiency of synchrotron emission is expected to be small, since the particles are accelerated along the magnetic field lines. Emission from accelerated particles is also expected to be strongly beamed along the field lines, which is inconsistent with the observed broad pulse profile in Figure 5.

Emission powered by accretion is a plausible mechanism. The standard model of accreting IPs involves an accretion column heated by the accretion shock and cooled by thermal

bremsstrahlung (Aizu 1973). It explains well the X-ray spectra of many IPs (see Cropper et al. 1999 for *Ginga* data, Suleimanov et al. 2005 for *RXTE*, Landi et al. 2009 for *Swift*/XRT and *INTEGRAL*/IBIS, Brunschweiger et al. 2009 for *Swift*/BAT, and Yuasa et al. 2010 for *Suzaku*). The main parameters of the model are the free-fall velocity $v_{\rm ff} = (2GM_{\rm WD}/R_{\rm WD})^{1/2}$ and the accretion rate per unit area, $a = \dot{M}/4\pi R_{\rm WD}^2 f$, where f is the fraction of the white dwarf surface occupied by the accretion column. The standard model assumes that the shock is radiative and pinned to the white dwarf surface, $h \ll R_{\rm WD}$. The shock altitude $h \lesssim v t_{\rm br}$, where $v = v_{\rm ff}/4 \sim 10^8$ cm s^{-1} is the postshock velocity of the accreting gas and $t_{\rm br} \sim 0.3/a$ s is the bremsstrahlung cooling timescale (with a expressed in units of g s^{-1} cm^{-2}). The net accretion rate $\dot{M}$ is determined from the X-ray luminosity $L_X = GM_{\rm WD}\dot{M}/R_{\rm WD}$.

This scenario would imply $\dot{M} \sim 2 \times 10^{14}$ g s^{-1} for AE Aqr, and the condition $a \gg 10^{-2}$ g s^{-1} cm^{-2} is satisfied if $f \ll 10^{-3}$. Such a small f may be possible if, e.g., the accretion flow in AE Aqr is concentrated in a thin wall of the accretion column (as Basko & Sunyaev 1976 suggested for accreting neutron stars). However, on the assumption of $M_{\rm WD} \sim 0.7\,M_\odot$ determined with the optical measurements (e.g., Watson et al. 2006; Echevarría et al. 2008), our calculations of the spectrum predicted by the standard accretion model do not provide a good fit for the *NuSTAR* data—the observed spectrum with the highest temperature of $9.3^{+6.1}_{-2.2}$ keV is softer than the predicted postshock temperature of 29 keV.

Two modifications might make the accretion model consistent with *NuSTAR* observations. (1) The shock altitude h in AE Aqr could be significant, perhaps even comparable to the white dwarf radius. Such tall accretion columns with low accretion rates were recently studied by Hayashi & Ishida (2014). The shallower gravitational potential at the high altitude results in a reduction of the postshock temperature below 20 keV typical of other IPs. The tall accretion column in AE Aqr was previously proposed as the source of the large hot spots on the white dwarf surface inferred from observations by the *Hubble* telescope (Eracleous et al. 1994) (2) The X-ray spectrum emitted by the accretion column could be affected by additional radiative losses due to cyclotron emission in the infrared band. Cyclotron emission is important when $B > 10^6$ G, and may carry away a significant part of the accretion column energy, especially at large altitudes where the plasma has the highest temperature. This effect could explain the relatively soft extended spectrum of AE Aqr above 3 keV. Detailed calculations of such models will be presented elsewhere.

In addition to the low X-ray luminosity and soft spectrum, AE Aqr has another special feature—weak absorption of soft X-rays, which corresponds to $N_{\rm H} < 8 \times 10^{21}$ cm^{-2}, lower than the $N_{\rm H} > 10^{22}$ cm^{-2} observed in many IPs (e.g., Ezuka & Ishida 1999; Yuasa et al. 2010). This feature could be explained by the lower density of the accretion column, and needs to be further investigated with detailed models. Also note that AE Aqr does not show evidence for a neutral (or weakly ionized) iron line. Among other IPs previously studied in the hard X-ray band, EX Hydrae has the lowest luminosity $L_X \sim 10^{32}$ erg s^{-1} and also the lowest column with $N_{\rm H} \lesssim 10^{22}$ cm^{-2} (Suleimanov et al. 2005). The shape of its 3–30 keV spectrum is not far from that of AE Aqr, although EX Hydrae is a nearly synchronous system with an orbital period of 98.3 min and a long spin period of 67.0 minutes (Belle et al. 2005), unlike AE Aqr.

The much smaller accretion rate of AE Aqr compared to many other IPs is thought to be due to the magnetic propeller effect (Wynn et al. 1997), whereby most of the mass lost by the secondary is being flung out of the binary by the magnetic field of the rapidly rotating white dwarf. Norton et al. (2004, 2008) performed numerical simulations of accretion flows in magnetic cataclysmic variables with wide ranges of magnetic moment, $\mu = 10^{32-36}$ G cm^3, and $P_{\rm spin}/P_{\rm orbit} = 10^{-3}$–1. They demonstrated that IPs with a very small ratio of $P_{\rm spin}/P_{\rm orbit} < 10^{-2}$ like AE Aqr ($P_{\rm spin}/P_{\rm orbit} = 9.3 \times 10^{-4}$) show magnetic propeller effects. Therefore, the tall accretion column could be formed in IPs with $P_{\rm spin}/P_{\rm orbit} < 10^{-2}$, though such systems would also be expected to have low X-ray luminosities, thus making them more challenging to identify. AE Aqr is the only currently known example. It is also possible that nearly synchronous systems similar to EX Hydrae could possess a tall accretion column. The low accretion rate in such systems is consistent with the picture of ring-like accretion discussed by Norton et al. (2008).

6. SUMMARY

We have analyzed X-ray data of the magnetized white dwarf AE Aqr observed with *NuSTAR* for 125 ks and *Swift* for 1.5 ks. The 0.5–30 keV spectra are well characterized by either an optically thin thermal plasma model with three temperatures with the highest temperature of $9.33^{+6.07}_{-2.18}$ keV, or an optically thin thermal plasma model with two temperatures plus a power-law component with photon index of $2.50^{+0.17}_{-0.23}$. The 3–20 keV pulse profile shows a sinusoidal modulation, with a pulsed fraction of $16.6\% \pm 2.3\%$. We find no evidence for the previously reported sharp feature in the pulse profile.

The observed soft X-ray spectrum with the broad pulse profile is hard to explain as a result of rotation-powered emission. Instead accretion-powered emission is more likely, although the observed spectrum is softer than predicted by the standard accretion column model. We suggest two modifications of the standard model to explain the AE Aqr spectrum: the shock altitude could be high, comparable to the white dwarf radius, and cyclotron emission with $B > 10^6$ G could additionally cool down the accretion plasma. Detailed calculations of such models will hopefully reproduce the spectrum and pulse profile of AE Aqr with the white dwarf mass consistent with that determined with the optical measurements.

This work was supported under NASA Contract No. NNG08FD60C, and made use of data from the *NuSTAR* mission, a project led by the California Institute of Technology, managed by the Jet Propulsion Laboratory, and funded by the National Aeronautics and Space Administration. We thank the *NuSTAR* Operations, Software and Calibration teams and the *Swift* Operations team for support with the execution and analysis of these observations. This research has made use of the *NuSTAR* Data Analysis Software (NuSTARDAS) jointly developed by the ASI Science Data Center (ASDC, Italy) and the California Institute of Technology (Caltech, USA) and the XRT Data Analysis Software (XRTDAS) developed under the responsibility of ASDC. T.K. was supported by Japan Society for the Promotion of Science (JSPS) Grant-in-Aid for Young Scientists (B) (No. 24740185).

Facilities: NuSTAR, *Swift*

REFERENCES

Aizu, K. 1973, PThPh, 49, 1184
Anders, E., & Grevesse, N. 1989, GeCoA, 53, 197

Basko, M. M., & Sunyaev, R. A. 1976, MNRAS, 175, 395
Belle, K. E., Howell, S. B., Mukai, K., et al. 2005, AJ, 129, 1985
Brunschweiger, J., Greiner, J., Ajello, M., & Osborne, J. 2009, A&A, 496, 121
Buccheri, R., Bennett, K., Bignami, G. F., et al. 1983, A&A, 128, 245
Burrows, D. N., Hill, J. E., Nousek, J. A., et al. 2005, SSRv, 120, 165
Choi, C.-S., & Dotani, T. 2006, ApJ, 646, 1149
Choi, C.-S., Dotani, T., & Agrawal, P. C. 1999, ApJ, 525, 399
Cropper, M., Wu, K., Ramsay, G., & Kocabiyik, A. 1999, MNRAS, 306, 684
de Jager, O. C., Meintjes, P. J., O'Donoghue, D., & Robinson, E. L. 1994, MNRAS, 267, 577
Echevarría, J., Smith, R. C., Costero, R., Zharikov, S., & Michel, R. 2008, MNRAS, 387, 1563
Eracleous, M., Horne, K., Robinson, E. L., et al. 1994, ApJ, 433, 313
Ezuka, H., & Ishida, M. 1999, ApJS, 120, 277
Friedjung, M. 1997, NewA, 2, 319
Fukazawa, Y., Mizuno, T., Watanabe, S., et al. 2009, PASJ, 61, 17
Gehrels, N., Chincarini, G., Giommi, P., et al. 2004, ApJ, 611, 1005
Gotthelf, E. V. 2003, ApJ, 591, 361
Harrison, F. A., Craig, W. W., Christensen, F. E., et al. 2013, ApJ, 770, 103
Hayashi, T., & Ishida, M. 2014, MNRAS, in press
Ikhsanov, N. R., & Beskrovnaya, N. G. 2012, ARep, 56, 595
Itoh, K., Okada, S., Ishida, M., & Kunieda, H. 2006, ApJ, 639, 397
Kaspi, V. M., Roberts, M. S. E., & Harding, A. K. 2006, in Compact Stellar X-Ray Sources, ed. W. Lewin & M. van der Klis (Cambridge: Cambridge Univ. Press), 279
Landi, R., Bassani, L., Dean, A. J., et al. 2009, MNRAS, 392, 630
Leahy, D. A., Elsner, R. F., & Weisskopf, M. C. 1983, ApJ, 272, 256
Mauche, C. W. 2006, MNRAS, 369, 1983
Mauche, C. W. 2009, ApJ, 706, 130
Mauche, C. W., Abada-Simon, M., Desmurs, J.-F., et al. 2012, MmSAI, 83, 651
Meintjes, P. J., de Jager, O. C., Raubenheimer, B. C., et al. 1994, ApJ, 434, 292
Norton, A. J., Butters, O. W., Parker, T. L., & Wynn, G. A. 2008, ApJ, 672, 524
Norton, A. J., Wynn, G. A., & Somerscales, R. V. 2004, ApJ, 614, 349
Oruru, B., & Meintjes, P. J. 2012, MNRAS, 421, 1557
Patterson, J. 1979, ApJ, 234, 978
Patterson, J. 1994, PASP, 106, 209
Patterson, J., Branch, D., Chincarini, G., & Robinson, E. L. 1980, ApJL, 240, L133
Smith, R. K., Brickhouse, N. S., Liedahl, D. A., & Raymond, J. C. 2001, ApJL, 556, L91
Suleimanov, V., Revnivtsev, M., & Ritter, H. 2005, A&A, 435, 191
Terada, Y., Hayashi, T., Ishida, M., et al. 2008, PASJ, 60, 387
Watson, C. A., Dhillon, V. S., & Shahbaz, T. 2006, MNRAS, 368, 637
Wilms, J., Allen, A., & McCray, R. 2000, ApJ, 542, 914
Wynn, G. A., King, A. R., & Horne, K. 1997, MNRAS, 286, 436
Yuasa, T., Nakazawa, K., Makishima, K., et al. 2010, A&A, 520, A25